Golden Plasmophores with Tunable Photoluminescence and Outstanding Thermal and Photothermal Stability

Mustafa Gharib, A. J. Yates, Stephen Sanders, Johannes Gebauer, Sebastian Graf, Anna Rosa Ziefuß, Nonappa, Günther Kassier, Christoph Rehbock, Stephan Barcikowski, Horst Weller, Alessandro Alabastri, Peter Nordlander,* Wolfgang J. Parak,* and Indranath Chakraborty*

Among various hybrid nanomaterials, the combination of plasmonic nanoparticles and fluorophores in a single multifunctional nanoplatform, so-called plasmophores, has attracted significant attention in different fields such as dark field, fluorescence, and photoacoustic imaging, biosensing, photothermal, and photodynamic therapy. Herein, author report a facile and controlled synthesis route of hybrid nanoplatforms composed of fluorescent gold nanoclusters (GNCs) coupled to plasmonic gold nanorods (GNRs) using controlled silica (SiO_2) dielectric spacers of different thicknesses from now on referred to as $GNR@SiO_2@GNC$ plasmophores. The results show different degrees of plasmon-enhanced fluorescence of the GNCs in their plasmophore hybrid system when placed at different distances from the plasmonic cores of the GNRs. On the other hand, these plasmophores show enhanced thermal stability compared to GNRs@CTAB (CTAB, cetyl trimethyl ammonium bromide). This results also demonstrated that upon annealing at elevated temperatures (800–1000 °C), the GNRs in the plasmophores are more thermally stable and robust than the GNRs@CTAB. More surprisingly, despite the commonly reported very low melting temperature of smaller-size nanocrystals, the GNCs in the plasmophores showed high thermal stability and do not exhibit significant structural changes at elevated temperatures (800–1000 °C).

1. Introduction

Hybrid or multifunctional nanomaterials are composed of more than one component in a single platform, and they may not only preserve the original features of each component but can also offer additional unique and beneficial features/functionalities for the resultant nanohybrid systems.[1,2] A classic example of the term "hybrid nanoparticle" originates from the late 1990s, when Zhou et al.[3] reported improved surface-enhanced Raman scattering (SERS) in Ag–TiO_2 core@shell hybrid nanostructures based on TiO_2 NPs upon amalgamation with Ag. Since then, a wide variety of hybrid plasmonic/fluorescent, plasmonic/magnetic, fluorescent/magnetic, and plasmonic/fluorescent/magnetic nanomaterials have been reported and have been used in a broad range of demonstrators/applications.[4–6] It has also been shown that the rational design of hybrid nanostructures allows them to maintain and even maximize the features and functions of their individual

M. Gharib, J. Gebauer, W. J. Parak, I. Chakraborty
Center for Hybrid Nanostructure (CHyN)
University of Hamburg
22761 Hamburg, Germany
E-mail: wolfgang.parak@uni-hamburg.de; indranath@iitkgp.ac.in

M. Gharib
Radiation Biology Department
Egyptian Atomic Energy Authority (EAEA)
Cairo 11787, Egypt

A. J. Yates, P. Nordlander
Department of Physics and Astronomy
Rice University
Houston, TX 77005, USA
E-mail: nordland@rice.edu

S. Sanders, A. Alabastri
Department of Electrical and Computer Engineering
Rice University
Houston, TX 77005, USA

S. Graf, H. Weller
Department of Chemistry
Universität Hamburg
20146 Hamburg, Germany

**ADVANCED
SCIENCE NEWS**

www.advancedsciencenews.com

**ADVANCED
OPTICAL
MATERIALS**

www.advopticalmat.de

nanocomponents.[2,7,8] Among various hybrid nanomaterials, the combination of plasmonic and fluorescence properties in a single multifunctional nanoplatform, the so-called plasmophores, has attracted great attention in different fields such as dark field, fluorescence, and photoacoustic imaging, biosensing, photothermal, and photodynamic therapy.[5,9–11] Such coupling of plasmonic nanoparticles (NPs) and inorganic/organic fluorophores has been studied as well in order to enhance the performance of those materials and to obtain higher quantum yields and photostable emitters for different applications.[12–18] For instance, there have been various reports on the modulation of the fluorescence quantum yield of quantum dots upon their coupling to plasmonic nanomaterials at different distances from the plasmonic cores.[19–22] Moreover, the fluorescence quantum yield as well as the photobleaching of many organic dyes have been modulated upon their coupling to plasmonic NPs at different distances from the plasmonic surface.[23–26]

Gold nanoclusters (GNCs) are noble metal-based fluorophores with ultrasmall size ($\approx$2 nm) in comparison to plasmonic gold nanoparticles that possess unique size-dependent photophysical properties induced by quantum confinement of the electrons. This motivates their applicability in various research areas including catalysis, and sensing, as well as in diverse biomedical applications.[27–30] Despite their commonly observed low photoluminescence (PL) quantum yield (QY)[31–33] compared to conventional fluorophores such as organic dyes and semiconductor quantum dots, GNCs have been reported to be photostable, water-soluble, and non-blinking, which makes them a fascinating choice of material for hybridization.[34–38] Som et al.,[39] have reported the synthesis of a hybrid material consisting of Ag nanoclusters and Te nanowires, which shows unusual bilayer assembly at the liquid–air interface. Chakraborty et al.,[40] have shown the assembly of different metal NCs on GNRs to form hybrid materials due to inter-NC hydrogen bonding. All these reports were focused on the assembly of metal nanoclusters induced by the ligands present on the NCs' surfaces. However, limited progress has been achieved with this type of hybrid materials beyond these distinct reports.

Herein we report a controlled synthesis of hybrid nanoplatforms, referred to as plasmophores, composed of fluorescent GNCs coupled to plasmonic GNRs via nanoscale electronically insulating silica (SiO$_2$) spacer layers of different thickness (GNR@SiO$_2$@GNC). Although a couple of recent reports

A. R. Ziefuß, C. Rehbock, S. Barcikowski
Department of Technical Chemistry I
University of Duisburg-Essen and Center for Nanointegration
Duisburg-Essen (CENIDE)
45141 Essen, Germany
Nonappa
Faculty of Engineering and Natural Sciences
Tampere University
Tampere FI 33720, Finland
G. Kassier
Max Planck Institute for the Structure and Dynamics of Matter
Geb. 99 (CFEL), Luruper Chaussee 149, 22761 Hamburg, Germany
I. Chakraborty
School of Nano Science and Technology
Indian Institute of Technology Kharagpur
Kharagpur, West Bengal 721302, India

have reported the synthesis of GNCs-conjugated GNRs hybrid systems,[41–44] some of them did not study the effect of distance between GNCs and GNRs on their physicochemical properties,[43,44] whereas for the other reports a very little was mentioned about the mechanisms via which the thermal and photothermal enhancement of both the fluorescent and plasmonic moiety takes place in such hybrid systems.

In this work, the influence of the silica shell thickness of the plasmophores on the thermal and photothermal behavior of GNCs and GNRs, as well as the fluorescence behavior of GNCs, was studied in detail. Functionalization of GNRs with SiO$_2$ shells enhances their colloidal stability, thermal/photothermal stability, as well as their photothermal efficiency. Moreover, conjugating the GNRs@SiO$_2$ with GNCs affects the fluorescence of the conjugated GNCs as a function of the SiO$_2$ thickness but also changes the mode of the photothermal reshaping of the GNRs upon ns laser irradiation.

2. Results and Discussion

2.1. Synthesis and Characterization of the Plasmophores

The CTAB-capped GNRs (GNRs@CTAB) were synthesized by the previously reported seed-mediated method, which involves using binary surfactant systems composed of CTAB and sodium oleate to obtain GNRs of different aspect ratios.[45] Three different approaches were employed to synthesize the nanohybrids. In the first approach, GNRs were conjugated with the GNCs via the direct electrostatic interaction between the positively charged GNRs@CTAB (ζ-potential = +39.2 ± 7.1 mV, Figure S6, Supporting Information) and the negatively charged glutathione-capped GNCs (GNCs@GSH) (ζ-potential = −32 ± 4.2 mV).[46] The second approach involved a layer-by-layer (LBL) assembly technique, during which GNRs@CTAB were coated with negatively charged poly(styrene sulfonate) (PSS) and positively charged poly(diallyldimethylammonium chloride) (PDADMAC) polyelectrolyte layers, respectively, and finally were incubated with the GNCs that attached via electrostatic attraction. However, in our experiments, these approaches either did not yield effective and homogeneous distributions of GNCs around the GNRs cores (first approach) or failed to conjugate the GNCs to the GNRs (second approach) (Figure S4, Supporting Information). Hence, we decided to coat our GNRs@CTAB with a silica (SiO$_2$) layer to obtain the GNRs@SiO$_2$ first and then conjugate them with the GNCs via ethyl dimethylaminopropyl carbodiimide/N-hydroxysuccinimide (EDC/NHS) coupling chemistry (**Figure 1**). The transmission electron microscopy (TEM) images of the nanohybrids obtained through the later approach ascertained the successful synthesis of the GNRs@SiO$_2$@GNCs plasmophores as could be revealed from the effective and homogeneous distribution of the GNCs around the GNRs@SiO$_2$ (Figure 1H–K). It is worth mentioning that our conjugation strategy is valid not only for conjugating GSH-coated GNCs to the GNRs@SiO$_2$ but also for conjugating other NCs such as bovine serum albumin-coated GNCs (GNCs@BSA) and dihydrolipoic acid-coated silver nanoclusters (SNCs@DHLA) (Figures S7–S9, Supporting Information). The UV–vis absorption spectra of the plasmophores did not exhibit spectral change, aggregation, or broadening of their plasmonic peaks (Figure S5, Supporting Information),

**ADVANCED
SCIENCE NEWS**

www.advancedsciencenews.com

**ADVANCED
OPTICAL
MATERIALS**
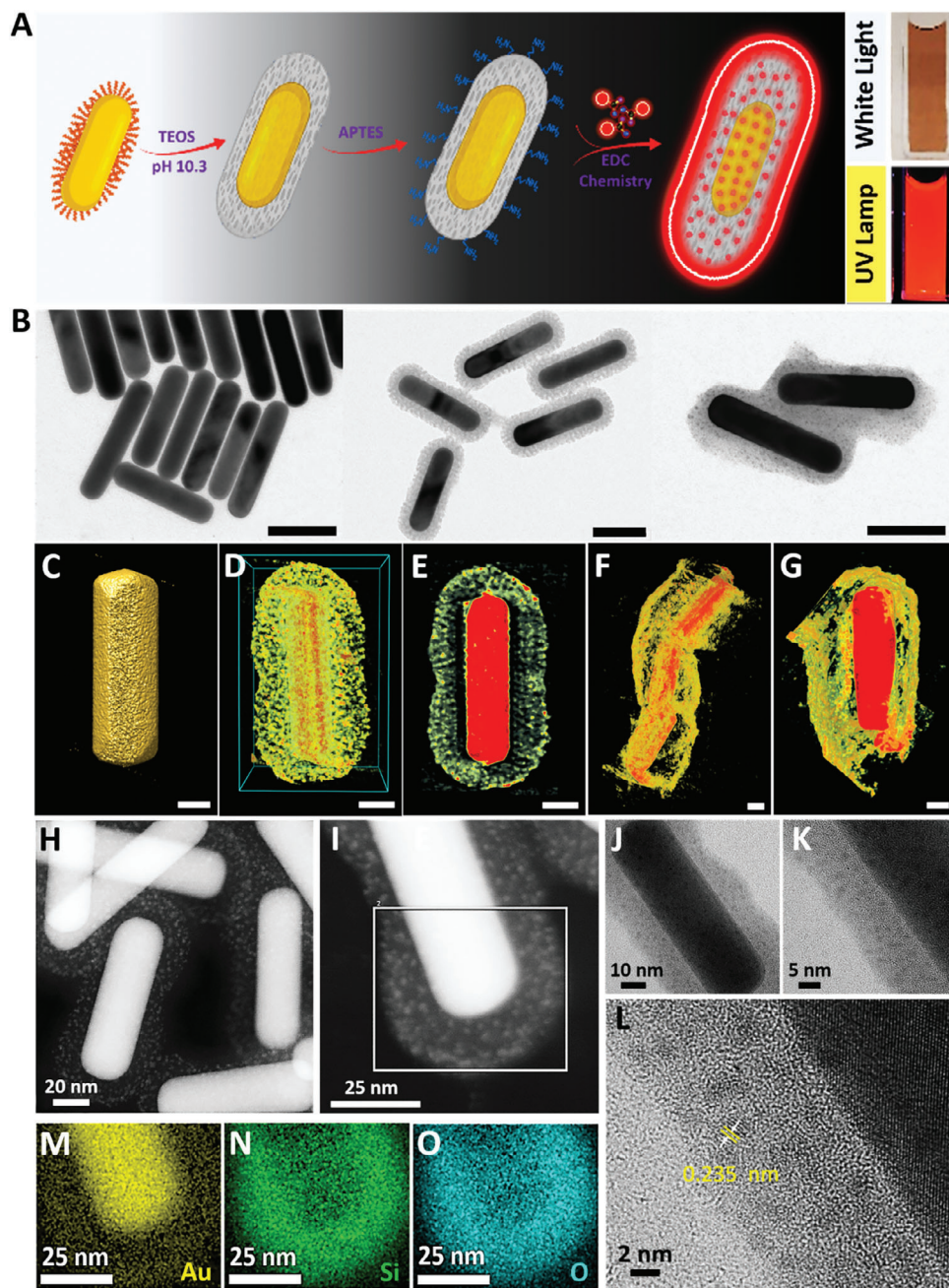
www.advopticalmat.de

Figure 1. Synthesis and characterization of GNRs@SiO₂@GNCs plasmophores. A) Schematic illustration of the synthetic route of the GNRs@SiO₂@GNCs plasmophores (left panel). Photographs of the plasmophores under white light and UV lamp excitation (right panel). B) TEM micrographs of GNRs@CTAB, GNRs@SiO₂, and GNRs@SiO₂@GNCs plasmophores (left to right, respectively) (scale bar = 50 nm). 3D reconstructured structures of C) GNRs@CTAB, D,E) GNRs@SiO₂, and its cross sectional view and F,G) GNRs@SiO₂@GNCs plasmophores and cross sectional view (scale bar = 20 nm). H,I) Dark-field TEM micrographs of GNRs@SiO₂@GNCs plasmophores. J–L) HR-TEM images of GNRs@SiO₂@GNCs. M–O) EDX elemental mapping of Au, Si, and O, respectively, in the GNRs@SiO₂@GNCs plasmophores.

whereas a significant broadening of the plasmonic peaks of both, GNRs@GNCs and GNRs@LBL@GNCs, was observed as compared to that of the original GNRs@CTAB (Figure S4, Supporting Information).

The SiO₂ shell thickness of the plasmophores was systematically tuned from ≈2.5 to 30 nm (2.5, 3.3, 4, 5, 6.5, 7.8, 8, 9.2, 13, 16, 20, 21.7, 23, 26, 28, and 30 nm) as revealed from the TEM im-

ages (Figures S2,S19,S20, Supporting Information). The coating of GNRs@CTAB with various thicknesses of SiO₂ was carried out using a modified Stöber method as reported previously.[47] Tuning the SiO₂ thickness was initiated by adjusting the CTAB concentration in the as-synthesized GNRs solution, which is a very crucial step to precisely control the silica shell thickness. The SiO₂ deposition started by the successive hydrolysis and

**ADVANCED
SCIENCE NEWS**

www.advancedsciencenews.com

**ADVANCED
OPTICAL
MATERIALS**

www.advopticalmat.de

condensation of the silica precursor, tetraethyl orthosilicate (TEOS), in alkaline reaction conditions on the CTAB micellar templates which are mostly around the GNRs surfaces. The SiO_2 shell thickness is determined by the ratio of silica deposited around the GNRs and freely formed silica in the solution as a function of the equilibrated CTAB added in the previous step.[47] Following this synthesis protocol, we successfully achieved the fabrication of a mesoporous silica shell with a pore size of 2.0–2.5 nm.[47–49]

The UV–vis absorption spectral features of different SiO_2 thickness-coated GNRs did not show aggregation or broadening of their plasmonic peaks (Figure S2, Supporting Information). Silanization of GNRs was accompanied by a small blue shift in the longitudinal surface plasmon resonance (LSPR) peak, which is attributed to the changes in refractive index as a result of CTAB removal during the purification steps in the synthesis of $GNRs@SiO_2$.[50] Our results are in agreement with a previous report that showed that the methanol used during the purification steps diffuses through the mesopores of the deposited silica layer and dissolves the underlying CTAB micellar templates.[50]

The conjugation of $GNRs@SiO_2$ of different SiO_2 thicknesses with the GNCs@GSH was carried out following two main steps. The $GNRs@SiO_2$ were first functionalized with amine groups via their interaction with 3-aminopropyl triethoxysilane (APTES). The terminal carboxylic groups of GNCs@GSH were then activated and made ready for their subsequent reaction with the primary amine-terminated $GNRs@SiO_2@APTES$ through the carbodiimide coupling chemistry. The GNCs@GSH with their activated carboxylic terminus were then conjugated to the amine-functionalized $GNRs@SiO_2$ via amide bond formation through the nucleophilic attack of primary amine groups of the latter on the activated carboxyl groups of the former. The successful functionalization of $GNRs@SiO_2$ with APTES and GNCs was confirmed by changes in zeta potential (ζ). The zeta potential of $GNRs@SiO_2$ was ≈−10 mV, and upon functionalization with APTES, it changed into ≈+9 mV and ultimately shifted to −6 mV after conjugation with the GNCs (Figure S6, Supporting Information). The full characterization of GNRs@CTAB before and after functionalization with SiO_2, APTES, and GNCs is depicted in Figure S6 (Supporting Information). Moreover, the successful conjugation of $GNRs@SiO_2$ with GNCs@GSH could be revealed from the TEM images which show a uniform distribution of the GNCs around the plasmonic cores (Figure 1). High resolution (HR)-TEM further confirms the homogeneous deposition of GNCs@GSH of 1.8 ± 0.35 nm average core diameter with a measured lattice fringes d-spacing of 0.235 nm, which matches well with reported values,[51] indicating the retained original crystallinity of the deposited GNCs (Figure 1L). Energy dispersive X-ray (EDX) elemental mapping of the plasmophores revealed a uniform SiO_2 deposition as well as an exclusive and preferential deposition of the GNCs at the outer surfaces of the plasmophore nanohybrid system (Figure 1M–O).To visualize the three diomenstional (3D) structures of GNRs, GNR@SiO2 and GNR@SIO2@GNCs, we performed transmission electron microscopy (TEM) tomographic resconstruction. Accodingly, a series of 2D TEM projections were collected and used to retrive the 3D structural details and internal structure of the hybrid systems. The electron tomography images of the plasmophores revealed the uniform and homogeneous distribution of GNCs

on the silica layer of the plasmophores without preferential spatial deposition and not within the mesoporous structure of the SiO_2 shells (Figure 1C–G). Moreover, a similar approach was successfully followed to conjugate ≈2 nm fluorophore to the surface of mesoporous silica-coated GNRs.[47] This in turn means that the GNCs (diameter ≈1.8 nm) are deposited at the same distance from the surfaces of the plasmonic cores ruling out the possibility of diffusing through the mesopores of the silica shell, especially with the expected additional pore size reduction of the pore size due to surface functionalization with APTES.[52,53] Moreover, both 2D and 3D TEM studies showed the formation of only a monolayer of the GNCs in the plasmophore nanohybrid system (Figure 1). These findings revealed that our conjugation strategy could be simply applied to deposit a monolayer of any carboxyl group-functionalized molecule/nanostructure to the plasmonic $GNRs@SiO_2$ nanostructures.

2.2. Distance-Dependent Fluorescence Properties of the Plasmophores

Notwithstanding the various attempts to investigate the plasmon-dependent fluorescence behavior of organic dyes,[54–59] inorganic QDs,[60–71] and fluorescent proteins,[72] when coupled to plasmonic GNRs, systematic studies of the separation dependence are missing. In order to investigate the separation-dependent fluorescence of the GNCs in the plasmophore nanohybrid system, we used steady-state fluorescence as well as the time-resolved photoluminescence (TRPL) for different aspect ratios (AR) GNRs. The distances between GNR and GNCs were controlled by varying the SiO_2 thicknesses (≈2.5–9.2 nm for high AR GNRs, and 13–30 nm for low AR GNRs). The results are presented in Figures S18–S20 (Supporting Information) including the characterizations of the plasmophores with different SiO_2 thickness. The steady-state fluorescence measurements revealed an obvious distance-dependent fluorescence enhancement of the GNCs. As could be seen from **Figure 2**, when the GNCs located at a distance of ≈2.5 and ≈9.2 nm from the surfaces of GNRs in high AR plasmophores they showed emission intensity ranged from minima (≈1.2 × 10⁶ CPS) to maxima (≈3.1 × 10⁶ CPS), whereas in low AR plasmophores (Figure S21, Supporting Information), when the GNCs located at a distance of ≈13 and ≈30 nm from the surfaces of GNRs they showed emission intensity ranged from minima (≈2.1 × 10⁴ CPS) to maxima (≈27.0 × 10⁴ CPS). Moreover, the steady-state fluorescence results showed that the metal/distance-dependent fluorescence of GNCs takes place without alteration in the emission spectral profiles of the GNCs, as could be revealed from their unchanged emission maxima (≈600 nm) and unaffected emission color upon excitation at 365 nm (Figure 2A; Figure S21, Supporting Information). This latter effect is of significance in various bioimaging applications where more than one single fluorophore is utilized, as any alterations in the emission spectral profile of one fluorophore could interfere with the spectral profiles of the other fluorophores.[73] Moreover, the metal/distant-dependent emission intensity of the GNCs follows a nonmonotonic behavior, where the emission intensity increases gradually until it reaches its maxima at a separation distance of ≈8 nm (high AR plasmophores) and ≈23 nm (low AR plasmophores)
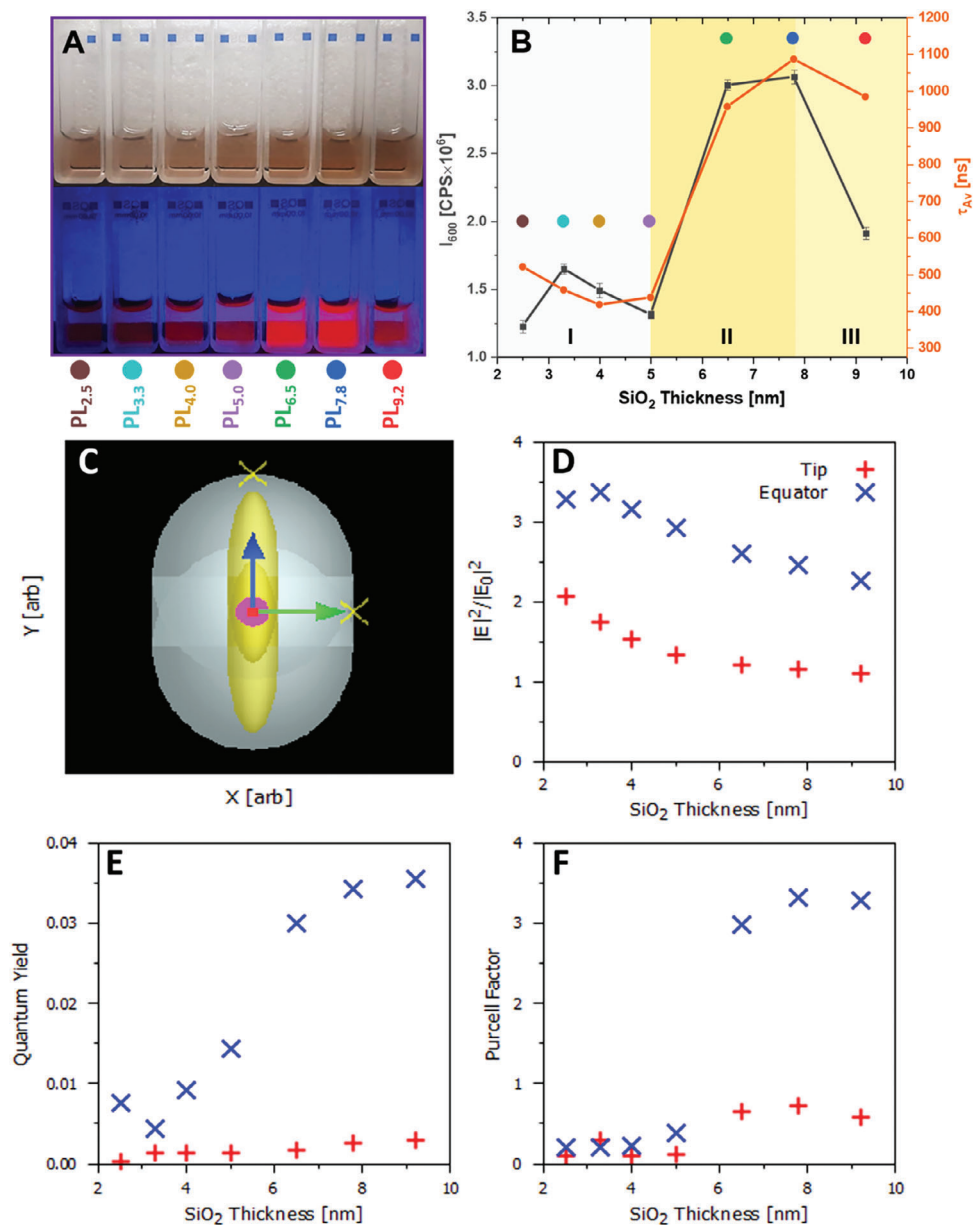
Figure 2. A) Photographs of high AR plasmophores of different silica thickness under white and UV-lamp excitation (PL = plasmophore, number indicates the thickness of silica shell in nm and its corresponding colored dot) and B) their respective steady-state fluorescence intensity and mean lifetime (Insets are cartoon illustrations of thin and thick plasmophores; the colored dots indicate the different samples, I-III indicates different regimes of distance-dependent fluorescence of plasmophores). C–F) Numerical estimation of fluorescence at the equator and the tip. (C) Schematic of the model used. The green arrow points to the equator, and the blue arrow points to the tip. (D) Excitation rate enhancement of the GNCs, as estimated by the square of the electric field enhancement at 365 nm. (E) The quantum yield of the GNCs at 600 nm, assuming 100% internal quantum yield. (F) Purcell factor of the GNCs at 600 nm on the surface of the silica layer.

and then drops back with increasing SiO_2 thickness (Figure 2B; Figure S21, Supporting Information). It is worth mentioning that in the case of high AR plasmophores an abrupt increase in the fluorescence intensity as well as fluorescence lifetime takes place when the silica thickness of the plasmophore changes from 5.0 to 6.5 nm (Figure 2B).

To understand the distance dependence of the plasmophore fluorescence, we modeled them using the Lumerical finite-difference time-domain software package.[74] Because particle

concentrations in the experiment are low, interactions between plasmophores are minimized, and we model the plasmophore as a single particle illuminated by a plane wave. Boundary conditions are shown schematically in Figure S49A,B (Supporting Information). The simulation consisted of two parts. In the first part, we modeled the $GNR@SiO_2$ complex with plane wave incoming light. We used this model to find the square of the electric field enhancement at the surface of the plasmophores, which is equal to the excitation rate enhancement in the unsaturated

**ADVANCED
SCIENCE NEWS**

www.advancedsciencenews.com

**ADVANCED
OPTICAL
MATERIALS**

www.advopticalmat.de

limit.[75,76] In the second part of the simulation, we replaced the plane wave source with a dipole emitter on the surface of the silica shell whose dipole moment points into the nanorod. This latter part of the simulation provided the quantum yield, which is the portion of the GNCs' energy that is radiated to the far field, and the Purcell factor, which is the ratio of the GNCs' radiative decay rate near the antenna to its decay rate in free space.[75] The quantum yield and Purcell factor were calculated in two locations: the tip, where the GNC couples most strongly to the GNR longitudinal plasmon resonance; and the equator, where the GNC couples most strongly to the transverse resonance of the GNR. We have assumed that the different plasmon modes of the GNCs do not couple and therefore can be simulated separately.

Figure 2 shows the results of the simulations for high-AR rods. The plasmophore is shown schematically in Figure 2C, where the green arrow points toward the equator, the blue arrow points to the tip, and the crosses represent the locations of particular GNCs. Figure 2D shows the square of the electric field enhancement at 365 nm, which again equals the excitation rate enhancement. Figure 2E,F show the quantum yield and the Purcell factor at 600 nm. The data in Figure 2F have been multiplied by a phenomenological arctangent function (details in the supplemental information), representing quenching, i.e. nonradiative relaxation of the emitter due to quantum mechanical effects. The figure shows that the GNR couples more strongly to emitters near the equator than to emitters near the tip. This is due to the transverse plasmon resonance at 550 nm (see Figures S18,S51, Supporting Information). Both, the excitation rate and the Purcell factor are strongly enhanced for emitters near the equator at wavelengths ≈550 nm. By contrast, emitters near the tip interact most strongly with light near the longitudinal plasmon resonance at 900 nm but do not couple strongly with the nanorod at wavelengths of 365 or 600 nm.

The distance-dependent emission enhancement of GNCs in the plasmophore nanohybrid system with its nonmonotonic trend could be explained as follows; at thinner SiO_2 spacer thickness, the drop in fluorescence intensity for GNCs that are located very close to the GNRs' surfaces is due to nonradiative quenching of the GNCs to the continuum states of the plasmonic GNRs.[47] Likewise, an obvious drop in the fluorescence intensity of GNCs takes place when the GNCs are placed far away from the plasmonic surfaces (i.e. at thicker SiO_2 spacer thickness), where the electric field generated by the GNRs and hence the spontaneous decay rate enhancement is minimal. The trade-off between the distant-dependent spontaneous decay rate enhancement and quenching will determine whether an enhancement or quenching will take place at a given GNCs-GNRs separation distance.[77] For a separation distance of ≈8 and 23 nm, in high and low AR plasmophores, the spontaneous decay rate enhancement considerably outweighs the quenching, resulting in a maximum fluorescence intensity. The distance-dependent fluorescence could be summarized as follows; strong fluorescence enhancement of the plasmophore system takes place when GNCs are located at certain distances (8 nm for high AR and 23 nm for low AR plasmophores) from the surfaces of the plasmonic GNRs. Here Förster Resonance Energy Transfer (FRET) to the GNRs is minimal and the plasmon-induced electric field still contributes to the excitation of GNCs (higher excitation rates due to strong local electromagnetic field) and/or emission enhancement of GNCs (higher emission rates due to enhancement of the radiative decay rates of the electromagnetically-coupled GNCs).[47,78,79] Considerable fluorescence quenching takes place in two limits: One limit is when FRET outweighs the enhancement of excitation and/or emission of the GNCs, which means that the excitations of the fluorophore dissipate efficiently in the plasmonic moiety. This effect could be seen clearly when GNCs are placed very close to the GNRs, ≈2.5 and 13 nm for high and low AR plasmophores, respectively. The second limit is when the contribution from the plasmon-enhanced electric field is minimal which occurs when the separations between GNCs and GNRs are large ≈9.2 and 30 nm in high and low AR plasmophores, respectively.[47]

It is worth noting that the concentrations of GNRs as well as GNCs were kept the same in all plasmophore systems as well as experimentally possible. Nevertheless, because of the different silica shell thicknesses in the obtained plasmophores, there may be an unequal amount of conjugated GNCs, i.e. with increasing the silica thickness one can expect an increase in the conjugated GNCs and vice versa. However, our results show an increased fluorescence from the intermediate-thickness plasmophores rather than from plasmophores of thicker silica thickness in both, our low and high AR plasmophores. Therefore, the data shows that the enhanced fluorescence is not an effect of the increased concentration of conjugated GNCs, but that distance from the plasmon surface plays a major role.

Time-resolved photoluminescence measurements were also carried out to determine the fluorescence lifetime of the GNCs as a function of their distance from the plasmonic surfaces of the GNRs in the plasmophore system. As could be seen from Figures S22,S23,S26,S27 (Supporting Information), the time-resolved fluorescence decay curves of the free GNCs as well as of the plasmophores follow a multiexponential decay and could be efficiently fitted with a triexponential decay function (details are added in SI). The fluorescence decay curves are consistent with the data obtained from the steady-state fluorescence measurements. As the distance between the plasmonic surfaces of GNRs and GNCs decreases, the fluorescence lifetime decreases, and the fluorescence decays faster (Figure 2B, regime I; Figure S24,S25,S28,S29, Supporting Information). This could be ascribed to the increased nonradiative decay rates commonly seen when the fluorophores get closer to the plasmonic surfaces.[47,80–82] On the other hand, when the GNCs are placed at a specific distance from the GNRs surfaces, the fluorescence decays slower and the fluorescence lifetime of the GNCs increases (Figure 2B, regime II; Figures S24,S25,S28,S29, Supporting Information). At such distances from the plasmonic core, there should be higher excitation rates of the GNCs as a result of the strong local electromagnetic field of the GNRs or from the enhanced emission of the GNCs by the enhanced radiative decay rates. When the GNCs are placed farther away from the GNRs, the radiative decay decreases and hence the fluorescence intensity as well as the fluorescence lifetime are lowered (Figure 2B, regime III). Our results are in good agreement with the observations reported by Abadeer et al.,[47] where the authors placed the IRDye 800CW DBCO at different distances from the plasmonic surfaces using dielectric silica spacer of different thicknesses and found a SiO_2 thickness-dependent fluorescence intensity in this fluorophore-plasmon coupling system and reported an approximate tenfold fluorescence enhancement of the IRDye when
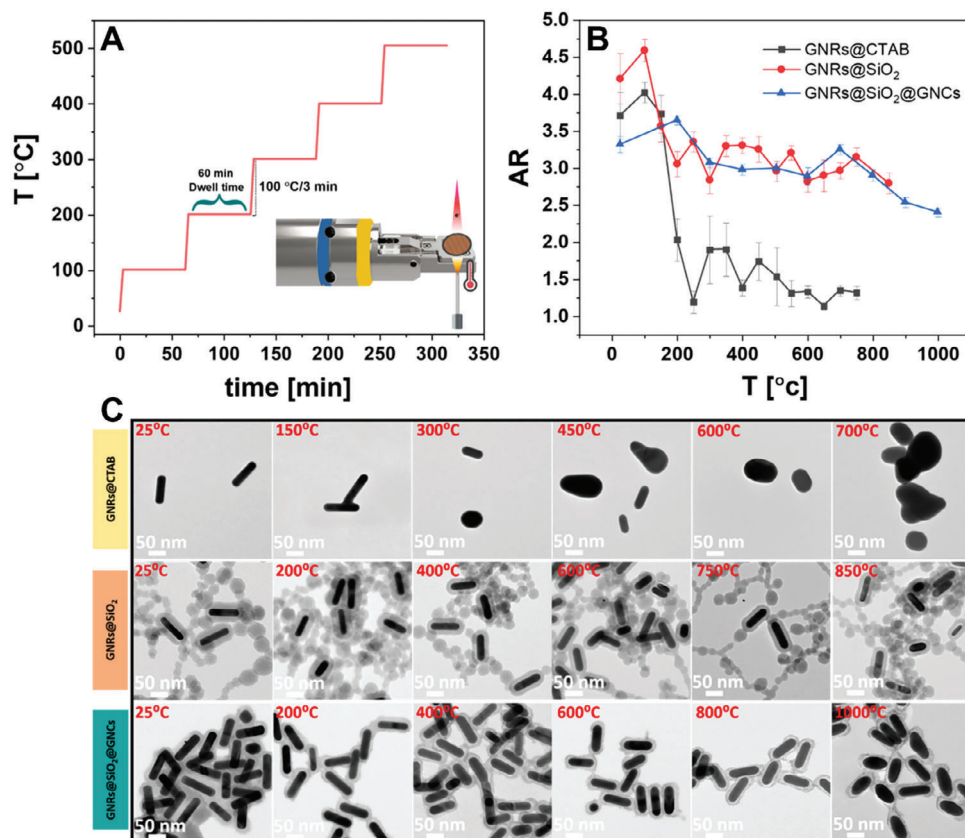
**ADVANCED
SCIENCE NEWS**

www.advancedsciencenews.com

**ADVANCED
OPTICAL
MATERIALS**

www.advopticalmat.de

Figure 3. In situ heating TEM study. A) Schematic illustration of the in situ thermal annealing TEM set-up. B) Effect of thermal annealing on the AR of GNRs@CTAB, GNRs@SiO$_2$, and GNRs@SiO$_2$@GNCs plasmophores. C) TEM images of in situ thermal annealing of GNRs@CTAB, GNRs@SiO$_2$, and GNRs@SiO$_2$@GNCs plasmophores at different temperatures.

placed at specific distance from the plasmonic surfaces of GNRs. The authors have also shown that decreasing the silica thickness results in a strong reduction in the fluorescence lifetime of the conjugated IRDye.

2.3. Thermal Stability of the Plasmophores

Conjugation of the GNRs@SiO$_2$ with the GNCs not only modulates the photophysical properties of the GNCs as discussed above but could also modulate the photophysical properties of the plasmonic GNRs cores. Thermal annealing of GNRs has been reported to induce drastic structural and morphological alterations of GNRs.[83] Many reports have shown that elevating the temperature of anisotropic NPs either thermally or via laser irradiation results in a loss of anisotropy, leaving behind deformed nanostructures of more stable crystal facets. Such behavior limits the use of these anisotropic NPs in many applications.[84–86] In order to study the thermal behavior of the GNRs in our plasmophore nanohybrid system, in situ TEM heating experiments were carried out. The heat-induced structural and morphological changes, as well as the melting process during the thermal annealing of GNRs@CTAB, GNRs@SiO$_2$, and GNRs@SiO$_2$@GNCs at different temperatures, were investigated using a TEM facility equipped with a special specimen

heating holder that allows for studying the heat-induced changes at significantly elevated temperature (1000 °C).

The in situ heating of CTAB-capped GNRs for temperatures below 150 °C did not affect their structure and morphology, and the GNRs@CTAB preserved their AR ($\approx$3.5) at such temperatures (**Figure 3**). As the temperature elevated to 150 °C, the GNRs started to develop some morphological changes, as could be revealed from the coalescence of the GNRs (Figure 3C). With the gradual increase of the annealing temperature, more structural transformations and distortions of the GNRs took place, resulting in more distorted and irregular nanostructures. When the annealing temperature reached 400 °C, the GNRs@CTAB started to transform almost completely into spherical-shaped nanostructures (Figure 3C). The almost complete transformation (observed at $\approx$505 °C), thus, took place hundreds of degrees below the melting temperature of bulk gold ($\approx$1064 °C)[87] (Figure S33, Supporting Information). Similar findings for in situ heat-induced GNR transformations have been previously reported.[88] Such thermal behavior of the CTAB-capped GNRs could be attributed to the inability of the CTAB layer to hinder the thermally-driven diffusion of the less stable gold surface atoms from the tips of the GNRs to their shaft. Such heat-induced surface atom diffusion dominates until complete morphological transformation into the more thermodynamically stable spherical NPs occurs. The in situ TEM annealing results showed enhanced thermal

**ADVANCED
SCIENCE NEWS**

www.advancedsciencenews.com

**ADVANCED
OPTICAL
MATERIALS**

www.advopticalmat.de

stability of GNRs@SiO₂ as could be revealed from their resistance to the heat-induced structural and morphological changes, even when they annealed at relatively high temperatures (850 °C) (Figure 3; Figure S34,S36, Supporting Information). Likewise, the in situ TEM results revealed the high thermal stability of the GNRs@SiO₂@GNCs plasmophores over the CTAB-coated GNRs (Figure 3B,C). The TEM images of the in situ TEM heating of our plasmophores showed the preserved anisotropic shape and AR of their core GNRs up to temperatures below 900 °C with some morphological changes started to emerge as the annealing temperature elevated to 900–1000 °C (Figure 3C; Figure S35, Supporting Information). At such a high temperature (900–1000 °C), which is very close to the bulk gold melting temperature (≈1064 °C), some of the GNRs started to transform into prolate spheroid- and Φ-shaped NPs. However, a complete morphological transformation of the GNRs into spherical NPs still, however, did not take place at such a higher annealing temperature. The enhanced thermal stability of GNRs in SiO₂-coated GNRs and the plasmophores compared to the CTAB-coated GNRs could be ascribed to one or more of the following mechanisms; 1) the rigidity of the silica shells prevents the heat-induced surface atoms diffusion and hence the thermally-driven structural rearrangement and morphological changes of GNRs, or 2) the SiO₂ layer provides an insulation/passivation barrier around the GNRs against the elevated temperatures which delays and maybe prevents surface atoms diffusion. It is worth noting that the agglomeration of particles seen in Figure 3 could be attributed to the drying effects that are usually seen during the processing of samples for TEM and it is not as a response to post-thermal treatment of the NPs.

To our surprise, the GNCs in the plasmophore hybrid system did not show significant structural transformations but rather exhibited excellent thermal stability at relatively high annealing temperatures (800–1000 °C), although some fusion of individual GNCs took place at 800 °C (Figure S35, Supporting Information). It is worth noting that the melting temperatures of gold NPs decrease as their size decreases,[89] and it has been reported that a gold nanocluster with a diameter of ≈2 nm has a melting temperature of as low as 127 °C and shows even a lower surface melting temperature.[90,91] This means that such incorporation of GNCs in a nanohybrid system such as in plasmophores enhances their thermal stability, making them more robust at hundreds of degrees higher annealing temperature than their original melting temperature. The enhanced thermal stability of GNCs in the plasmophores could be ascribed to the strong binding as well as anchoring of the GNCs to the silica support which in turn suppresses GNCs diffusion and hence their sintering and coalescence at elevated annealing temperatures.

The thermal stability of GNRs, GNCs, and plasmophores was assessed by recording their UV–vis absorption as well as their PL spectra before and after annealing their solutions at elevated temperatures. The UV–vis data showed a blue-shift of the LSPR peak of the GNRs upon annealing at 100 °C, whereas, no obvious change in the LSPR peak position for plasmophores (Figure S38A, Supporting Information). These results are consistent with the solid-state in situ TEM heating experiment. On the other hand, the PL data shows no difference between the PL stability of GNCs and plasmophores upon annealing at 100 °C (Figure S38B,C, Supporting Information). The diminished fluorescence of both free GNCs as well as plasmophores upon thermal anneal-

ing may be due to lower charge transfer between GSH and GNCs which could be attributed to temperature-induced weakening of the Au—S bonds.[92]

2.4. Photothermal Stability of the Plasmophores

Apart from the thermal heating-induced structural and morphological changes of GNRs, laser photothermal heating of GNRs could also induce fragmentation and melting of the GNRs.[86,93–95] The latter effect has been used to control the size and shape of many nanostructures as well as to obtain highly monodispersed NPs.[94,96–99] Various efforts have been devoted to enhancing the photothermal stability of many NPs in diverse applications where NPs are required to be exposed to laser irradiation for extended periods of time, such as cancer photothermal ablation. Inspired by their robust structures and thermal stability, we decided to evaluate the photothermal behavior of the plasmophores during their irradiation with ns laser pulses, which will initiate the local heating of the NP surface. The photothermal stability of different AR plasmophores (AR ≈ 3.5 and 5.5, λ_{LSPR} ≈ 785 and 900 nm, respectively) after being irradiated with different ns laser pulses (200–9000 pulses) using the first harmonic of an Nd:YAG ns-laser source (1064 nm, 320 mJ cm⁻²) was evaluated by recording their UV–vis absorption spectra as well as by analyzing their morphological and structural changes in TEM. The UV–vis absorption spectra of ns laser-irradiated CTAB-capped GNRs (AR ≈ 3.5 and 5.5) showed a photothermally-induced spectral hole-burning as could be revealed from the diminished extinction values at λ_{LSPR} with a concomitant increase of the extinction values at λ_{TSPR} (Figure S39A,S41A, Supporting Information). It is worth noting that the transient increase in the extinction maxima and reduction of spectral bandwidth at λ_{LSPR} after irradiating the high AR GNRs@CTAB (≈5.5) with ≈500–1000 ns laser pulses arise from the ability of such laser beams to minimize the polydispersity of GNRs, which in turns reduces their spectral bandwidth and increases their extinction maxima at λ_{LSPR}. Our results agree with previous work that shows the ability to synthesize highly monodisperse GNRs with ultranarrow LSPR spectral bandwidth.[100] Irradiating different AR GNRs@CTAB with 9000 ns laser pulses brings about dramatic morphological and structural changes and leads finally to the almost complete loss of rod-shaped nanostructure and the dominance of the more thermodynamically stable spherical-shaped NPs (**Figure 4**; Figures S40,S42, Supporting Information). In order to figure out the mechanism of the laser-induced photothermal reshaping of GNRs, TEM imaging of larger GNRs@CTAB (AR ≈ 5.5) was carried out at intermediate laser pulses (200–3000 pulses). The TEM results showed the formation of intermediate nanostructures at moderate laser pulses (200–3000 pulses), such as the Φ-shaped NPs, where the length of GNRs diminishes, and their shafts become thicker, along with other bent and twisted nanostructures (Figure S42, Supporting Information). Such structures are believed to dominate at an early stage of laser irradiation of NPs due to the photothermal heating-induced planar defects and twin formation in the GNRs.[86,101] Based on the aforementioned findings, one could conclude that the ns laser-induced reshaping of GNRs@CTAB follows a melting-mediated mechanism (Scheme S1, Supporting Information). It
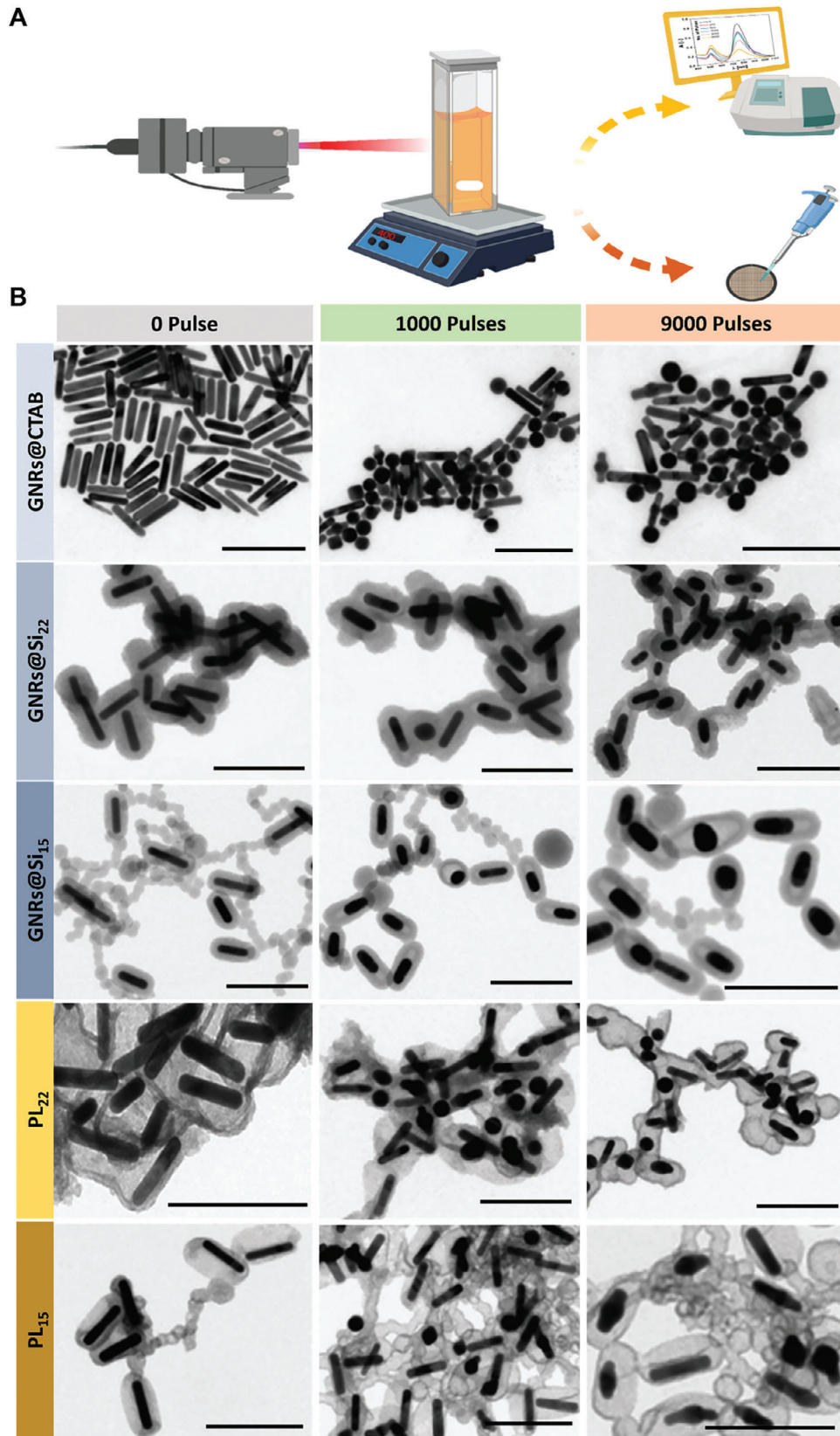
**ADVANCED
SCIENCE NEWS**

www.advancedsciencenews.com

**ADVANCED
OPTICAL
MATERIALS**

www.advopticalmat.de

Figure 4. In situ plasmon-mediated reshaping of GNRs. A) Schematic illustration of the photothermal heating experiment set-up. B) TEM images of photothermal heating using different ns laser pulses of GNRs@CTAB, different silica thickness GNRs@SiO$_2$ (Si$_{22}$ and Si$_{15}$, numbers indicate different

has been shown that the laser irradiation-induced structural and morphological changes of GNRs@CTAB take place due to the increased kinetic energy of gold atoms upon photothermal heating which in turn results in their surface diffusion. The continuous absorption of laser light by the GNRs results in increased lattice energy, and more surface diffusion takes place until a more thermodynamically stable spherical structure dominates.[93,101] It is worth noting that the densely-packed CTAB on the surfaces of GNRs has a significantly lower thermal conductivity (K) than that of water ($K_{CTAB} = 0.140$ W mK^{-1} and $K_{Water} = 0.598$ W mK^{-1}),[102] which means that the CTAB layer acts as a barrier against heat diffusion upon laser radiation, leading to a subsequent heat accumulation and accelerates the photothermal-induced morphological and structural changes.

However, the UV–vis absorption spectroscopic and TEM imaging results showed enhanced photothermal stability of the SiO_2-coated GNRs (Figure S39B,C, Supporting Information). In this experiment, GNRs were coated with different SiO_2 shell thicknesses (GNRs@Si$_{22}$ and GNRs@Si$_{15}$, Si$_{22}$, and Si$_{15}$ indicate SiO_2 thickness in nm). Coating the lower AR GNRs (≈ 3.5) with either Si$_{22}$ or Si$_{15}$ shells renders them more photothermally stable, as could be revealed from their nearly unaffected UV–vis spectral features (Figure S39B,C, Supporting Information), and that the GNRs become more resistant to the photothermal-induced structural and morphological changes when coated with thicker SiO_2 shells. The TEM results confirm the photothermal stability of low AR GNRs@SiO$_2$ (Figure S40, Supporting Information). Closer examination of the TEM images of GNRs@Si$_{15}$ irradiated with 9000 ns laser pulses revealed that the photothermally-induced reshaping of GNRs@SiO$_2$ takes place in a different way than that of GNRs@CTAB. The TEM imaging and UV–vis results show a clear shortening and decrease of the AR of GNRs@SiO$_2$ as well as a hypsochromic shift of their LSPR band, respectively, which reveals that the photothermal reshaping of GNRs@SiO$_2$ most probably follows a fragmentation-mediated mechanism rather than a melting-based mechanism (Scheme S1, Supporting Information). Furthermore, the formation of bullet-shaped NPs upon photothermal heating of GNRs@SiO$_2$ revealed that the reshaping proceeds via a fragmentation mechanism where a gradual release of fragmented gold takes place through the mesopores of the SiO_2 shells (Figure S40 and Scheme S1, Supporting Information). Our results are consistent with previous findings.[103–105] In order to gain further insight into the origin of the photothermal stability of SiO_2-coated GNRs, we performed numerical simulations to predict the temperature reached by GNRs@CTAB, GNRs@SiO$_2$, and plasmophores for both high and low AR geometries. We found that GNRs coated in SiO_2 shells reached higher temperatures, due to the red shift of their resonances leading to a larger absorption cross section at the laser wavelength (see Figure S49, Supporting Information). Therefore, we ascribed the enhanced photothermal stability of SiO2-coated GNRs to the rigid structure of the SiO_2 shells that hinders the diffusion of surface atoms and the concomitant photothermal reshaping of GNRs. The same findings were also exhibited by SiO_2-coated

larger GNRs (≈ 5.5) (Figures S41B,C,S43,S44, Supporting Information). It is worth mentioning that the diminished photothermal stability of higher AR GNRs@SiO$_2$ compared to lower AR GNRs@SiO$_2$ is likely due to a combination of two effects: 1) the higher absorption cross-section of high AR GNRs@SiO$_2$ at the laser wavelength (1064 nm) compared to that of the low AR GNRs@SiO$_2$, which means more energy deposition on the larger GNRs@SiO$_2$,[84] and 2) the considerable thermodynamic stability of shorter GNRs@SiO$_2$ compared to larger GNRs@SiO$_2$ that makes them more resistant to the photothermal-induced morphological and structural changes,[84] giving that both NPs are irradiated using the same laser parameters.

The UV–vis absorption data and the TEM images of the GNRs@SiO$_2$@GNCs plasmophores irradiated with different pulses ns laser showed that functionalization of GNRs@SiO$_2$ with GNCs switches their photothermal reshaping behavior from a fragmentation-mediated into a melting-mediated process (Scheme S1, Supporting Information). These findings could be clearly seen from the spectral hole burning of the plasmophores at their LSPR band (Figures S39D,E,S41D,E, Supporting Information), as well as the formation of Φ-shaped NPs and bent nanostructures (Figure 4, Figures S45,S46, Supporting Information) upon irradiation with different pulses of ns laser. As such, the photothermal reshaping process of our plasmophores resembles that of GNRs@CTAB, although the rate of spectral changes and melting kinetics of our plasmophores are much slower as well as their morphological transformation and structural rearrangement are not as fast and drastic as that of GNRs@CTAB. It is worth noting that the agglomeration of particles seen in Figure 4 could be attributed to the drying effects that are usually seen during the processing of samples for TEM and it is not as a response to post-photothermal treatment of the NPs.

It should be pointed out that the fluorescence behavior of GNCs in our plasmophore nanohybrid system was not affected or quenched upon irradiation with frequent ns laser pulses for an extended time (**Figure 5**). HR-TEM images of our GNRs@SiO$_2$@GNCs plasmophores did not reveal any structural changes or melting of the fluorescent GNCs (Figure 5). Such high thermal (vide supra) and photothermal stability of the GNCs in our nanohybrid system could be of great importance in various applications.

In order to gain further insight into the photothermal stability displayed by the plasmophores, we performed finite element method (FEM) simulations with the commercial software COMSOL Multiphysics (details in the supplemental information). We show the plasmophore geometry and resulting electric field enhancement under longitudinal polarization in **Figure 6A,B**. In the second step, the pulse profile was assumed to have a Gaussian distribution in time with a width of 9 ns. Figure 6C shows the temperature of the nanorod as a function of time for the different high AR systems for different SiO_2 shell thicknesses (Si22 and Si15), as it was in Figures S39,S41 (Supporting Information). This plot shows two important pieces of information that determine the photothermal reshaping properties of the plasmophores—the maximum temperature increase, as well as

---

SiO_2 thickness in nm), and GNRs@SiO$_2$@GNCs plasmophores of different silica thickness (PL$_{22}$ and PL$_{15}$, PL = plasmophore, number indicates the thickness of silica shell in nm). Scale bar = 200 nm.
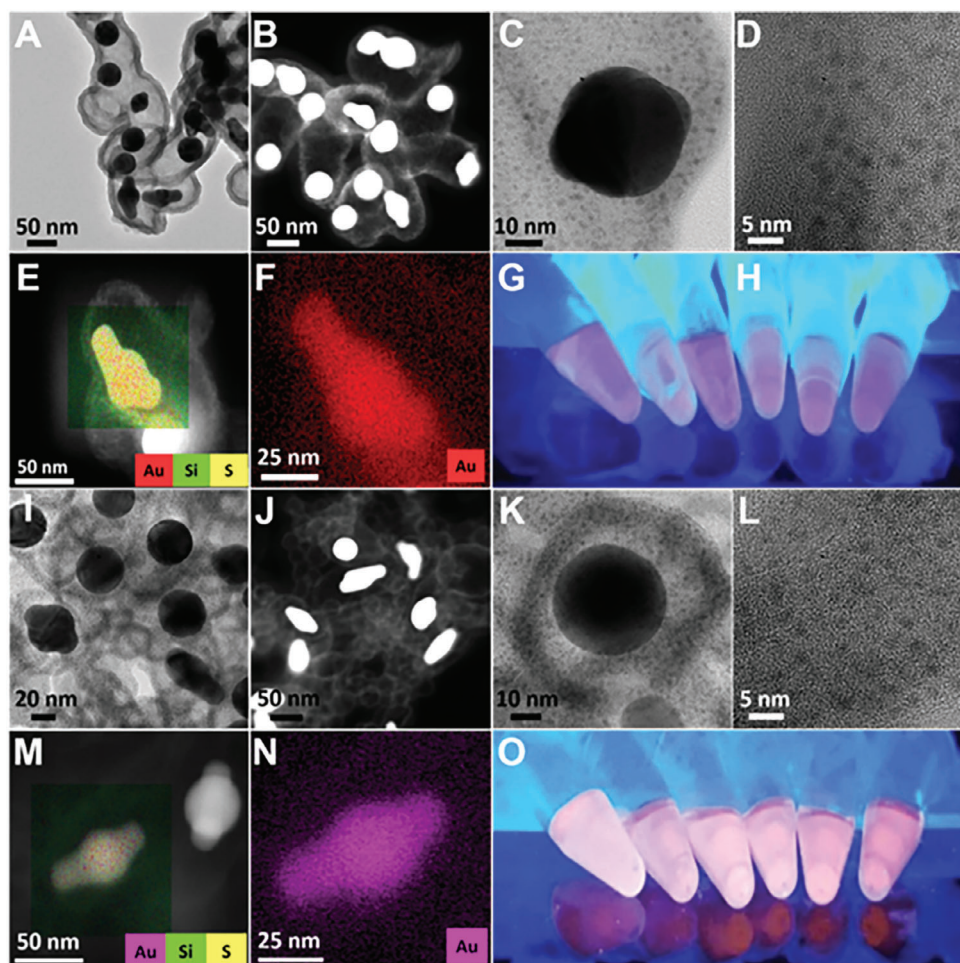
Figure 5. High photothermal stability of GNCs in the GNRs@SiO$_2$@GNCs plasmophores after irradiation with 9000 ns laser pulses of ≈320 mJ cm^{-2} fluence. A and I) Bright-field TEM images of PL$_{22}$ and PL$_{15}$, respectively. B and J) Dark-field TEM images of PL$_{22}$ and PL$_{15}$, respectively. C, D and K, L) HR-TEM of PL$_{22}$ and PL$_{15}$, respectively. E and M) EDX mapping of Au, Si, and S in PL$_{22}$ and PL$_{15}$, respectively. F and N) EDX mapping of Au in PL$_{22}$ and PL$_{15}$, respectively. G and O) Photographs of PL$_{22}$ and PL$_{15}$, respectively, under UV-lamp excitation.

the duration over which the temperature increase is maintained. We observe that the dynamics are very similar between all of the systems, and therefore, in Figure 6D, we plot only the maximum temperature increase reached for all of the plasmophores. We see that the temperature increase in the low AR systems is smaller than for the high AR systems. This is because the absorption peak of the low AR systems occurs at smaller wavelengths (see Figures S18,S49 for the experimental and numerical spectra, respectively, Supporting Information), further away from the laser wavelength of 1064 nm. Furthermore, we observe that the bare nanorods reach a lower temperature than those coated in SiO$_2$. Therefore, we attribute the thermal stability of the latter to the rigid structure of the SiO$_2$ layer inhibiting the surface diffusion of gold atoms of the nanorod.

3. Conclusion

We have shown a facile route for the synthesis of plasmophores composed of fluorescent GNCs conjugated to plasmonic GNRs using dielectric silica spacers. The silica shell thickness could

be tuned by controlling the free CTAB micellar concentration in the GNRs solution. Tuning the silica layer thickness allows for placing our GNC fluorophores at determined distances either closer to or further away from the GNR plasmonic cores. The results showed that our plasmophores have higher colloidal stability in different media compared to CTAB-coated GNRs. Moreover, our plasmophores showed more enhanced physicochemical properties of both plasmonic GNRs and the GNC fluorophores. The results showed a nonmonotonic trend for fluorescence enhancement due to two competing processes, nonradiative fluorescence quenching at small GNCs-GNRs separation distance and fluorescence-enhancing radiation decay from the strong electric field near the surfaces of the plasmonic GNRs. The best separation distance of the GNCs was shown to be ≈8 and 23 nm for high and low AR plasmophores, respectively, where the increase in spontaneous decay rate outweighs the nonradiative quenching. On the other hand, our plasmophores showed more enhanced thermal stability compared to the CTAB-coated GNRs. Although the melting temperature of smaller-size nanocrystals is very low (127 °C for 2 nm Au nanocrystals), to our surprise, at ele-
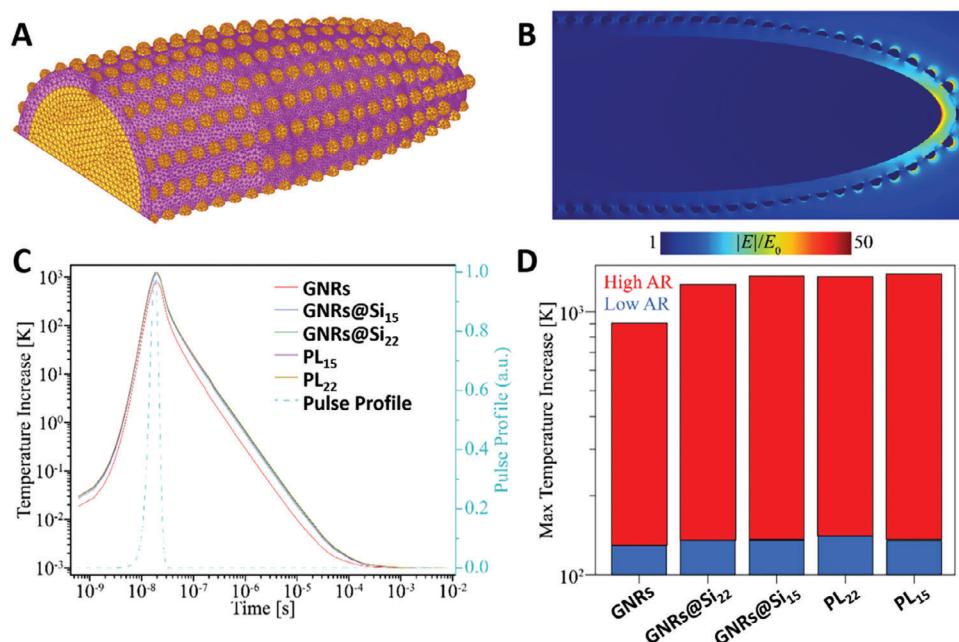
Figure 6. Photothermal simulations of plasmophores in water. A) Geometry and mesh of a high AR plasmophore with a SiO_2 shell thickness of 2.5 nm. The yellow and pink colors show gold and SiO_2 domains, respectively. B) Electric field enhancement of the plasmophore when illuminated by light with a wavelength of 1064 nm polarized along its axis. C) Temperature increase of the high AR nanorods, GNRs@SiO_2 (GNRs@Si15 and GNRs@Si22), and GNRs@SiO_2@GNCs plasmophores (PL15 and PL22) as a function of time when illuminated with the first harmonic of a 9 ns Nd:YAG laser at a fluence of 320 mJ cm^{-2}. D) Maximum temperature increase reached by different AR plasmophores.

vated temperatures (800–1000 °C) the GNCs in the plasmophores did not exhibit significant morphological changes and showed high thermal stability. Furthermore, our plasmophores showed apparent photothermal stability compared to CTAB-coated GNRs and this stability is enhanced by increasing the silica layer thickness. The laser irradiation of our plasmophores did not affect the shape or the fluorescence behavior of the GNCs. Our GNRs@SiO_2@GNCs plasmophores hold promise for diverse applications such as multiplexed imaging, and PTT, and the high surface area of silica coating facilitates efficient drug loading capability. The surfaces of the silica-coated GNRs and GSH-capped GNCs in the plasmophore make them potential candidates for many biomedical applications. Furthermore, the metal/plasmon-enhanced fluorescence exhibited by our system may be of benefit for many low-quantum yield fluorophores and thus could improve the detection limits of fluorophore-based sensors.

The current study, while providing valuable insights into the controlled synthesis of GNR@SiO_2@GNC plasmophores and their applications, acknowledges certain limitations that warrant consideration. Achieving consistent and precise control over the silica shell thickness, although reported as controlled in this work, may pose challenges in scalability and reproducibility. The findings are specific to the chosen combination of GNRs and fluorescent nanoclusters, and caution should be exercised when extending these results to different plasmonic nanoparticles or fluorophores. Furthermore, the exploration of biocompatibility for in vivo applications is lacking in this study, necessitating future investigations into the potential cytotoxicity and suitability of plasmophores in biological systems. Future work to broaden the understanding and practical implementation of such plas-

mophores such as conducting comprehensive biological studies and functionalizing the plasmophore surface for targeted applications should be considered. Additionally, exploring multimodal imaging and quantifying the enhancement of quantum yields for low-quantum yield fluorophores are areas that can significantly contribute to the broader understanding and application of this hybrid nanoplatform.

Supporting Information

Supporting Information is available from the Wiley Online Library or from the author.

Acknowledgements

Conflict of Interest

The authors declare no conflict of interest.

Data Availability Statement

The data that support the findings of this study are available in the supplementary material of this article.

Keywords

fluorescence, gold nanoclusters, gold nanorods, plasmophores, thermal stability

[1] M. B. Cortie, A. M. McDonagh, *Chem. Rev.* **2011**, *111*, 3713.

[2] S. Zong, Z. Wang, R. Zhang, C. Wang, S. Xu, Y. Cui, *Biosens. Bioelectron.* **2013**, *41*, 745.

[3] Y. Zhou, C. Y. Wang, H. J Liu, Y. R. Zhu, Z. Y. Chen, *Mater. Sci. Eng., B* **1999**, *67*, 95.

[4] N. C. Bigall, W. J. Parak, D. Dorfs, *NanoToday* **2012**, *7*, 282.

[5] A. Saha, S. Basiruddin, R. Sarkar, N. Pradhan, N. R. Jana, *J. Phys. Chem. C* **2009**, *113*, 18492.

[6] J. Zhang, G. Qi, C. Xu, Y. Jin, *Anal. Chem.* **2019**, *91*, 14074.

[7] B. H. Jun, M. S. Noh, J. Kim, G. Kim, H. Kang, M. S. Kim, Y. T. Seo, J. Baek, J. H. Kim, J. Park, S. Kim, *Small* **2010**, *6*, 119.

[8] M. S. Noh, B.-H. Jun, S. Kim, H. Kang, M.-A. Woo, A. Minai-Tehrani, J.-E. Kim, J. Kim, J. Park, H.-T. Lim, S.-C. Park, T. Hyeon, Y.-K. Kim, D. H. Jeong, Y.-S. Lee, M.-H. Cho, *Biomaterials* **2009**, *30*, 3915.

[9] B. Dubertret, M. Calame, A. J. Libchaber, *Nat. Biotechnol.* **2001**, *19*, 365.

[10] F. Jia, X. Liu, L. Li, S. Mallapragada, B. Narasimhan, Q. Wang, *J. Control. Rel.* **2013**, *172*, 1020.

[11] G. A. Sotiriou, *Wiley Interdiscip. Rev.: Nanomed. Nanobiotechnol.* **2013**, *5*, 19.

[12] F. Y. Song, P. S. Tang, H. Durst, D. T. Cramb, W. C. W. Chan, *Angew. Chemie Int. Ed.* **2012**, *51*, 8773.

[13] G. Lozano, S. R. Rodriguez, M. A. Verschuuren, J. G. Rivas, *Light: Sci. Appl.* **2016**, *5*, e16080.

[14] G. Lozano, D. J. Louwers, S. R. Rodríguez, S. Murai, O. T. Jansen, M. A. Verschuuren, J. G. Rivas, *Light: Sci. Appl.* **2013**, *2*, e66.

[15] X. Gu, T. Qiu, W. Zhang, P. K. Chu, *Nanoscale Res. Lett.* **2011**, *6*, 1.

[16] T. Ming, H. Chen, R. Jiang, Q. Li, J. Wang, *J. Phys. Chem. Lett.* **2012**, *3*, 191.

[17] S. Chandra, et al., *Sol. Energy Mater. Sol. Cells* **2012**, *98*, 385.

[18] Q. Wu, L. Chen, L. Huang, J. Wang, J. Liu, C. Hu, H. Han, *Biosens. Bioelectron.* **2015**, *74*, 16.

[19] B. Ji, E. Giovanelli, B. Habert, P. Spinicelli, M. Nasilowski, X. Xu, N. Lequeux, J.-P. Hugonin, F. Marquier, J.-J. Greffet, B. Dubertret, *Nat. Nanotechnol.* **2015**, *10*, 170.

[20] S. Jin, E. DeMarco, M. J. Pellin, O. K. Farha, G. P. Wiederrecht, J. T. Hupp, *J. Phys. Chem. Lett.* **2013**, *4*, 3527.

[21] M. T. Zin, K. Leong, N.-Y. Wong, H. Ma, M. Sarikaya, A. K.-Y. Jen, *Nanotechnology* **2008**, *20*, 015305.

[22] D. Nepal, L. F. Drummy, S. Biswas, K. Park, R. A. Vaia, *ACS Nano* **2013**, *7*, 9064.

[23] A. Riedinger, F. Zhang, F. Dommershausen, C. Röcker, S. Brandholt, G. U. Nienhaus, U. Koert, W. J. Parak, *Small* **2010**, *6*, 2590.

[24] G. P. Acuna, M. Bucher, I. H. Stein, C. Steinhauer, A. Kuzyk, P. Holzmeister, R. Schreiber, A. Moroz, F. D. Stefani, T. Liedl, F. C. Simmel, P. Tinnefeld, *ACS Nano* **2012**, *6*, 3189.

[25] S. Pal, P. Dutta, H. Wang, Z. Deng, S. Zou, H. Yan, Y. Liu, *J. Phys. Chem. C* **2013**, *117*, 12735.

[26] S. L. Capehart, M. P. Coyle, J. E. Glasgow, M. B. Francis, *J. Am. Chem. Soc.* **2013**, *135*, 3011.

[27] G. Li, R. Jin, *J. Am. Chem. Soc.* **2014**, *136*, 11347.

[28] H. Li, W. Zhu, A. Wan, L. Liu, *Analyst* **2017**, *142*, 567.

[29] I. Chakraborty, T. Pradeep, *Chem. Rev.* **2017**, *117*, 8208.

[30] N. Kaur, R. N. Aditya, A. Singh, T.-R. Kuo, *Nanoscale Res. Lett.* **2018**, *13*, 1.

[31] T. Q. Yang, B. Peng, B.-Q. Shan, Y.-X. Zong, J.-G. Jiang, P. Wu, K. Zhang, *Nanomaterials* **2020**, *10*, 261.

[32] A. R. Ziefuss, T. Steenbock, D. Benner, A. Plech, J. Göttlicher, M. Teubner, B. Grimm-Lebsanft, C. Rehbock, C. Comby-Zerbino, R. Antoine, D. Amans, I. Chakraborty, G. Bester, M. Nachev, B. Sures, M. Rübhausen, W. J. Parak, S. Barcikowski, *Adv. Mater.* **2021**, *33*, 2101549.

[33] Y. Zeng, S. Havenridge, M. Gharib, A. Baksi, K. L. D M. Weerawardene, A. R. Ziefuß, C. Strelow, C. Rehbock, A. Mews, S. Barcikowski, M. M. Kappes, W. J. Parak, C. M. Aikens, I. Chakraborty, *J. Am. Chem. Soc.* **2021**, *143*, 9405.

[34] S. Chakraborty, S. Babanova, R. C. Rocha, A. Desireddy, K. Artyushkova, A. E. Boncella, P. Atanassov, J. S. Martinez, *J. Am. Chem. Soc.* **2015**, *137*, 11678.

[35] M. Wu, Z. Li, J. Yao, Z. Shao, X. Chen, *ACS Biomater. Sci. Eng.* **2019**, *5*, 4799.

[36] M. H. Griep, J. D. Demaree, D. P. Cole, T. C. Henry, S. P. Karna, *Plasmonics* **2020**, *15*, 897.

[37] M. Li, Y.-H. Lao, R. L. Mintz, Z. Chen, D. Shao, H. Hu, H.-X. Wang, Y. Tao, K. W. Leong, *Nanoscale* **2019**, *11*, 2631.

[38] J. Xia, X. Wang, S. Zhu, L. Liu, L. Li, *ACS Appl. Mater. Interfaces* **2019**, *11*, 7369.

[39] A. Som, I. Chakraborty, T. A. Maark, S. Bhat, T. Pradeep, *Adv. Mater.* **2016**, *28*, 2827.

[40] A. Chakraborty, A. C. Fernandez, A. Som, B. Mondal, G. Natarajan, G. Paramasivam, T. Lahtinen, H. Häkkinen, Nonappa, T. Pradeep, *Angew. Chem., Int. Ed.* **2018**, *57*, 6522.

[41] Q. Duan, M. Yang, B. Zhang, Y. Li, Y. Zhang, X. Li, J. Wang, W. Zhang, S. Sang, *J. Photochem. Photobiol., B* **2021**, *215*, 112111.

[42] O. Pavelka, K. Kvakova, J. Vesely, J. Mizera, P. Cigler, J. Valenta, *Nanoscale* **2022**, *14*, 3166.

[43] R. V. Nair, M. F. Puthiyaparambath, R. Chatanathodi, L. V. Nair, R. S. Jayasree, *Nanoscale* **2022**, *14*, 13561.

[44] X. Su, B. Fu, J. Yuan, *Mater. Lett.* **2017**, *188*, 111.

[45] X. Ye, C. Zheng, J. Chen, Y. Gao, C. B. Murray, *Nano Lett.* **2013**, *13*, 765.

[46] A. M. Alkilany, A. Alsotari, M. Y. Alkawareek, S. R. Abulateefeh, *Sci. Rep.* **2019**, *9*, 1.

[47] N. S. Abadeer, M. R. Brennan, W. L. Wilson, C. J. Murphy, *ACS Nano* **2014**, *8*, 8392.

[48] J. E. van der Hoeven, T.-S. Deng, W. Albrecht, L. A. Olthof, M. A. van Huis, P. E. de Jongh, A. van Blaaderen, *ACS Omega* **2021**, *6*, 7034.

[49] S. Zhou, H. Sha, B. Liu, X. Du, *Chem. Sci.* **2014**, *5*, 4424.

[50] L. R. Rowe, B. S. Chapman, J. B. Tracy, *Chem. Mater.* **2018**, *30*, 6249.

[51] C. Wang, Y. Hu, C. M. Lieber, S. Sun, *J. Am. Chem. Soc.* **2008**, *130*, 8902.

[52] N. Kamarudin, A. A. Jalil, S. Triwahyono, N. F. M. Salleh, A. H. Karim, R. R. Mukti, B. H. Hameed, A. Ahmad, *Microporous Mesoporous Mater.* **2013**, *180*, 235.

[53] S. B. Hartono, W. Gu, F. Kleitz, J. Liu, L. He, A. P. J. Middelberg, C. Yu, G. Q. (M.) Lu, S. Z. Qiao, *ACS Nano* **2012**, *6*, 2104.

**ADVANCED
SCIENCE NEWS**

www.advancedsciencenews.com

**ADVANCED
OPTICAL
MATERIALS**

www.advopticalmat.de

[54] A. Kinkhabwala, Z. Yu, S. Fan, Y. Avlasevich, K. Müllen, W. E. Moerner, *Nat. Photonics* **2009**, *3*, 654.

[55] F. Tam, G. P. Goodrich, B. R. Johnson, N. J. Halas, *Nano Lett.* **2007**, *7*, 496.

[56] R. Bardhan, N. K. Grady, J. R. Cole, A. Joshi, N. J. Halas, *ACS Nano* **2009**, *3*, 744.

[57] Y. Chen, K. Munechika, D. S. Ginger, *Nano Lett.* **2007**, *7*, 690.

[58] Y. Fu, J. Zhang, J. R. Lakowicz, *J. Am. Chem. Soc.* **2010**, *132*, 5540.

[59] T. Ming, L. Zhao, Z. Yang, H. Chen, L. Sun, J. Wang, C. Yan, *Nano Lett.* **2009**, *9*, 3896.

[60] O. Kulakovich, N. Strekal, A. Yaroshevich, S. Maskevich, S. Gaponenko, I. Nabiev, U. Woggon, M. Artemyev, *Nanoletters* **2002**, *2*, 1449.

[61] M. Barth, S. Schietinger, S. Fischer, J. Becker, N. Nüsse, T. Aichele, B. Löchel, C. Sönnichsen, O. Benson, *Nano Lett.* **2010**, *10*, 891.

[62] X. Ma, H. Tan, T. Kipp, A. Mews, *Nano Lett.* **2010**, *10*, 4166.

[63] P. P. Pompa, L. Martiradonna, A. D Torre, F. D Sala, L. Manna, M. De Vittorio, F. Calabi, R. Cingolani, R. Rinaldi, *Nat. Nanotechnol.* **2006**, *1*, 126.

[64] A. Bek, R. Jansen, M. Ringler, S. Mayilo, T. A. Klar, J. Feldmann, *Nano Lett.* **2008**, *8*, 485.

[65] M. Schmelzeisen, Y. Zhao, M. Klapper, K. Müllen, M. Kreiter, *ACS Nano* **2010**, *4*, 3309.

[66] J.-H. Song, T. Atay, S. Shi, H. Urabe, A. V. Nurmikko, *Nano Lett.* **2005**, *5*, 1557.

[67] P. Viste, J. Plain, R. Jaffiol, A. Vial, P. M. Adam, P. Royer, *ACS Nano* **2010**, *4*, 759.

[68] K. Leong, Y. Chen, D. J. Masiello, M. T. Zin, M. Hnilova, H. Ma, C. Tamerler, M. Sarikaya, D. S. Ginger, A. K.-Y. Jen, *Adv. Funct. Mater.* **2010**, *20*, 2675.

[69] H. M. Gong, L. Zhou, X.-R. Su, S. Xiao, S.-D. Liu, Q.-Q. Wang, *Adv. Funct. Mater.* **2009**, *19*, 298.

[70] K. Munechika, Y. Chen, A. F. Tillack, A. P. Kulkarni, I. J.-L. Plante, A. M. Munro, D. S. Ginger, *Nano Lett.* **2010**, *10*, 25982603.

[71] M. Bauch, K. Toma, M. Toma, Q. Zhang, J. Dostalek, *Plasmonics* **2014**, *9*, 781.

[72] J. E. Donehue, E. Wertz, C. N. Talicska, J. S. Biteen, *J. Phys. Chem. C* **2014**, *118*, 15027.

[73] L. Zhao, T. Ming, H. Chen, Y. Liang, J. Wang, *Nanoscale* **2011**, *3*, 3849.

[74] Lumerical Solutions, I, https://www.ansys.com/products/optics/fdtd (accessed: February, 2024).

[75] L. Novotny, B. Hecht, *Principles of Nano-Optics*, Cambridge University Press, Cambridge, **2012**.

[76] P. Anger, P. Bharadwaj, L. Novotny, *Phys. Rev. Lett.* **2006**, *96*, 113002.

[77] B. Fu, J. D. Flynn, B. P. Isaacoff, D. J. Rowland, J. S. Biteen, *J. Phys. Chem. C* **2015**, *119*, 19350.

[78] C. D. Geddes, J. R. Lakowicz, *J. Fluoresc.* **2002**, *12*, 121.

[79] N. Gandra, C. Portz, L. Tian, R. Tang, B. Xu, S. Achilefu, S. Singamaneni, *Angew. Chem., Int. Ed.* **2014**, *53*, 866.

[80] P. Reineck, et al., *ACS Nano* **2013**, *7*, 6636.

[81] X. Li, et al., *Appl. Phys. Lett.* **2009**, *94*, 063111.

[82] N. N. Horimoto, K. Imura, H. Okamoto, *Chem. Phys. Lett.* **2008**, *467*, 105.

[83] Y. Wang, S. Teitel, C. Dellago, *Nano Lett.* **2005**, *5*, 2174.

[84] A. B. Taylor, A. M. Siddiquee, J. W. Chon, *ACS Nano* **2014**, *8*, 12071.

[85] S. Inasawa, M. Sugiyama, Y. Yamaguchi, *J. Phys. Chem. B* **2005**, *109*, 3104.

[86] S. Link, C. Burda, B. Nikoobakht, M. A. El-Sayed, *J. Phys. Chem. B* **2000**, *104*, 6152.

[87] Y. Li, et al., *Sci. Rep.* **2015**, *5*, 1.

[88] Y. Khalavka, C. Ohm, L. Sun, F. Banhart, C. Sönnichsen, *J. Phys. Chem. C* **2007**, *111*, 12886.

[89] Y. Wang, C. Dellago, *J. Phys. Chem. B* **2003**, *107*, 9214.

[90] P. Buffat, J. P. Borel, *Phys. Rev. A* **1976**, *13*, 2287.

[91] P. Borisyuk, et al., *Meas. Techn.* **2010**, *53*, 128.

[92] Y.-T. Wu, C. Shanmugam, W.-B. Tseng, M. M. Hiseh, W.-L. Tseng, *Nanoscale* **2016**, *8*, 11210.

[93] S. Link, C. Burda, M. B. Mohamed, B. Nikoobakht, M. A. El-Sayed, *J. Phys. Chem. A* **1999**, *103*, 1165.

[94] S.-S. Chang, C.-W. Shih, C.-D. Chen, W.-C. Lai, C. R. C. Wang, *Langmuir* **1999**, *15*, 701.

[95] S. Link, C. Burda, B. Nikoobakht, M. A. El-Sayed, *Chem. Phys. Lett.* **1999**, *315*, 12.

[96] T. Wenzel, J. Bosbach, A. Goldmann, F. Stietz, F. Träger, *Appl. Phys. B* **1999**, *69*, 513.

[97] H. Kurita, A. Takami, S. Koda, *Appl. Phys. Lett.* **1998**, *72*, 789.

[98] A. Takami, H. Kurita, S. Koda, *J. Phys. Chem. B* **1999**, *103*, 1226.

[99] J. Bosbach, et al., in *Laser Applications in Microelectronic and Optoelectronic Manufacturing IV*, International Society for Optics and Photonics, Washington **1999**.

[100] G. González-Rubio, P. Díaz-Núñez, A. Rivera, A. Prada, G. Tardajos, J. González-Izquierdo, L. Bañares, P. Llombart, L. G. Macdowell, M. Alcolea Palafox, L. M. Liz-Marzán, O. Peña-Rodríguez, A. Guerrero-Martínez, *Science* **2017**, *358*, 640.

[101] G. González-Rubio, A. Guerrero-Martínez, L. M. Liz-Marzán, *Acc. Chem. Res.* **2016**, *49*, 678.

[102] Y. Horiguchi, K. Honda, Y. Kato, N. Nakashima, Y. Niidome, *Langmuir* **2008**, *24*, 12026.

[103] Y.-S. Chen, et al., *Opt. Express* **2010**, *18*, 8867.

[104] A. Plech, V. Kotaidis, M. Lorenc, J. Boneberg, *Nat. Phys.* **2006**, *2*, 44.

[105] W. Albrecht, T.-S. Deng, B. Goris, M. A. van Huis, S. Bals, A. van Blaaderen, *Nano Lett.* **2016**, *16*, 1818.